ACS APPLIED MATERIALS & INTERFACES

Research Article

www.acsami.org

Construction of Cellulose Based ZnO Nanocomposite Films with Antibacterial Properties through One-Step Coagulation

Feiya Fu,[†] Lingyan Li,[†] Lianjie Liu,[‡] Jun Cai,[‡] Yaping Zhang,[§] Jinping Zhou,*[,†] and Lina Zhang[†]

[†]Department of Chemistry and Key Laboratory of Biomedical Polymers of Ministry of Education, Wuhan University, Luojia Hill, Wuhan 430072, China

[‡]Hubei Provincial Cooperative Innovation Center of Industrial Fermentation and Key Laboratory of Fermentation Engineering (Ministry of Education), Hubei University of Technology, Wuhan 430068, China

[§]State Key Laboratory Cultivation Base for Nonmetal Composites and Functional Materials, Southwest University of Science and Technology, Mianyang, 621010, China

ABSTRACT: Cellulose based ZnO nanocomposite (RCZ) films were prepared from cellulose carbamate−NaOH/ZnO solutions through one-step coagulation in Na_2SO_4 aqueous solutions. The structure and properties of RCZ films were characterized using XRD, FTIR, XPS, SEM, TEM, TG, tensile testing, and antibacterial activity tests. The content of ZnO in RCZ films was obtained in the range of 2.7−15.1 wt %. ZnO nanoparticles with a hexagonal wurtzite structure agglomerated into large particles, which firmly embedded in the cellulose matrix. RCZ films displayed good mechanical properties and high thermal stability. Moreover, the films exhibited excellent UV-blocking properties and antibacterial activities against *Staphylococcus aureus* and *Escherichia coli*. A dramatic reduction in viable bacteria was observed within 3 h of exposure, while all of the bacteria were killed within 6 h. This work provided a novel and simple pathway for the preparation of regenerated cellulose films with ZnO nanoparticles for application as functional biomaterials.

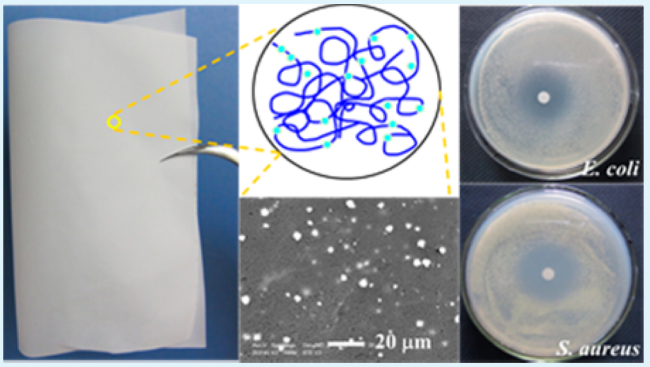

KEYWORDS: *cellulose, ZnO nanoparticles, nanocomposite film, one-step coagulation, antibacterial*

INTRODUCTION

ZnO is an important multifunctional semiconductor material that possesses a wide direct band gap of 3.37 eV and a high excitation binding energy of 60 meV.[1] It is widely utilized as a material in semiconductors, optical devices, piezoelectric devices, surface acoustic wave devices, sensors, transparent electrodes, solar cells, and antibacterial activity, etc.[2−5] In recent years, there have been widespread reports on the synthesis of ZnO nanoparticles and nanostructures using physical and chemical methods, with efforts to control the morphology, size, and shape.[6,7] Coating suitable substrates with ZnO nanoparticles provides further potential applications for functional materials in various fields.[8−10]

As a linear 1,4-β-glucan, cellulose is the most abundant renewable natural polymer on earth and a promising raw material in the chemical and biological industries.[11] Cellulose products, such as paper, regenerated cellulose (RC) films, and nonwoven fibers, have many advantages including chemical stability, biocompatibility, biodegradability, and good mechanical properties.[12] They have been used extensively in the fields of membrane separation, pharmaceuticals, cosmetics, and the food industry.[11,12] Recently, there has been increased interest in the use of nanofibrillated cellulose for the production of nanocomposites containing inorganic nanoparticles.[13−16] However, there have thus far been few reports concerning the fabrication of ZnO coated cellulose matrix.[17−31] In one instance, Alejandro et al. reported a simple mixing process using a high energy mixer/mill machine under high pressure (750 MPa).[22] Through a common papermaking process, nanofibrillated cellulose coated with 1.21−2.28 wt % ZnO was prepared with good antibacterial properties. Unfortunately, direct mechanical mixing methods can only obtain microscale interaction between ZnO and cellulose matrix, leading to poor mechanical properties.[24] Different carbohydrates (glucose, sucrose, alginate, and starch) have thus been employed as capping agents to facilitate the adhesion of ZnO nanoparticles onto the surface of cellulose fibers.[21] Chemical methods, such as precipitation and sol−gel approaches, have shown some distinct advantages over physical methods, including the morphology control of ZnO and inexpensive equipment.[6,7,17−19] The synthesis is generally performed in an alcohol or alkaline solution, and zinc salts such as $ZnCl_2$,[25] $Zn(NO_3)_2$,[10,18,19,26] and $Zn(Ac)_2$[5,17,30−34] are used as starting materials. Cellulose in the form of fibers, paper, bacterial

Received: November 2, 2014
Accepted: January 8, 2015
Published: January 8, 2015

 © 2015 American Chemical Society

DOI: 10.1021/am507639b
ACS Appl. Mater. Interfaces 2015, 7, 2597−2606

Scheme 1. Preparation of RCZ Films from Cellulose Carbamate−NaOH/ZnO Solution through One-Step Coagulation in aq Na_2SO_4

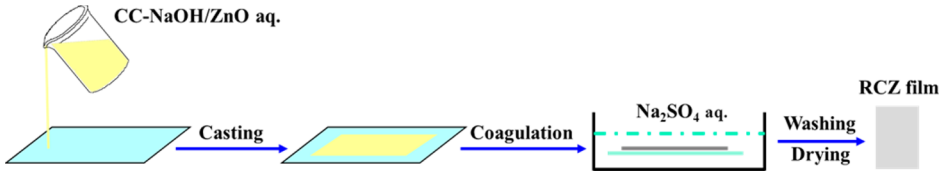

cellulose, and cotton fabrics are immersed into the precursor solution, and nano- and microstructures grow directly on the matrix. During the coating process, the reaction mixture should be maintained at a high temperature (ca. 90−150 °C) for a period of 3−20 h, allowing for the complete conversion of zinc salts to ZnO. The process requires repetition on some occasions to improve the adhesion of ZnO seed layer.[18,26] Most recently, ZnO nanocrystallites were grown in situ on cellulose nanofibers through a combination of electrospinning and solvothermal techniques.[20,27] The obtained hybrid nanofibers exhibited strong photocatalytic efficiency and antibacterial activity but poor mechanical strength and low production capacity. To the best of our knowledge, there has only one report of cellulose/ZnO nanocomposite obtained directly from cellulose solution because cellulose cannot be dissolved in common solvents due to its strong intermolecular and intramolecular hydrogen bonds.[23]

In our previous work, a green method was developed for the preparation of RC multifilament and films from cellulose carbamate (CC).[35−37] CC was first efficiently prepared using microwave heating; it was then dissolved in NaOH/ZnO aqueous solutions through a freezing−thawing process. Finally, the CC dope was coagulated in an acid bath to provide RC fibers and films, and ZnO was transformed to zinc salt, which subsequently washed off from the cellulose matrix. Further research into the construction of cellulose nanocomposites remaining zinc compound from the CC-NaOH/ZnO solution would be highly valuable. In the present work, cellulose based ZnO nanocomposite (RCZ) films were prepared from CC-NaOH/ZnO solutions through one-step coagulation in aqueous of Na_2SO_4. The morphology, structure, and physicochemical properties of the films were comprehensively investigated. ZnO nanoparticles were firmly embedded in the cellulose matrix, resulting in the excellent UV-blocking and antibacterial properties of the films. The process was advantageous in the low cost of raw materials and the relative ease for ZnO nanocomposites constructing while also avoiding the addition of any other toxic substances.

EXPERIMENTAL SECTION

Materials. The cellulose sample (cotton linter pulp) was supplied by Hubei Chemical Fiber Co. Ltd. (Xiangyang, China). The degree of polymerization (DP) was determined as 800. In addition, ZnO, NaOH, and Na_2SO_4 of analytical grade were purchased from Sinopharm Chemical Reagent Co., Ltd. (Shanghai, China) and used without further purification.

Microwave Synthesis of CC. CC samples were prepared in accordance with the method outlined in previous work.[38,39] Cellulose was immersed into a 45 wt % urea aqueous solution. The mixture was then stood at ambient temperature for 1 h, which was followed by dehydration, separation, and oven drying. The obtained mixture of cellulose/urea was subsequently heated in a microwave oven (Whirlpool, VIP 273F, 850 W, 10 levels) at 425 W for 12−15 min. Finally, the sample was washed with water and vacuum-dried. The DP, nitrogen content (*N*%), and degree of substitution (DS) of the CC sample were determined as 660, 1.44%, and 0.17, respectively.

Preparation of RCZ Films. NaOH/ZnO aqueous solution was prepared by mixing 7 wt % NaOH, 0−1.6 wt % ZnO and distilled water in accordance with our previous work.[36] CC was dispersed into a NaOH/ZnO solution, which was then cooled to −12 °C. The frozen mixture was subsequently thawed at room temperature, and a transparent CC solution was obtained. As shown in Scheme 1, the CC solution with a concentration of 5.5 wt % was cast on a glass board to give a thickness of 0.5 mm and subsequently coagulated in 15 wt % Na_2SO_4 solutions at 50 °C for 15 min. The coagulated films were then transferred into distilled water to remove NaOH and Na_2SO_4. The nanocomposite films were coded as RCZ4, RCZ8, RCZ12, and RCZ16, according to the concentrations of ZnO in the solvent (0.4, 0.8, 1.2, and 1.6 wt %, respectively). RC films were prepared from CC-7 wt % NaOH solutions by the same way.

Characterization. The intrinsic viscosity ($[\eta]$) of cotton linter and CC in cadoxen was measured at 25 ± 0.1 °C. The DP was calculated from $[\eta]$ according to the Mark−Houwink equation.[35] The nitrogen content of the CC pulp was determined using an elemental analyzer (CHN-O-RAPID, Heraeus Co., Germany). FT-IR spectra were performed on a FTIR spectrometer (NICOLET 5700, Thermo Electron Co., USA). The test specimens were prepared using the KBr-disk method. The samples were cut into powder and then vacuum-dried at 40 °C for 24 h before measurements. The UV−vis spectra of the films were recorded on a UV-6100PCS (MAPADA, China) double beam spectrophotometer in the range of 200−800 nm with a resolution of 2 nm. The water contact angle was measured and calculated using the dynamic mode on a Data Physics instrument (OCA20). One drop of water (2 μL) was placed onto the surface of the films using an automatic piston syringe and subsequently photographed. Thermogravimetric (TG) analysis was applied on a NETZSCH STA449*c*/3/G thermal analyzer (NETZSCH, Germany). The primary thermograms were recorded in a temperature range from ambient to 800 °C at a heating rate of 10 °C/min under an air atmosphere.

X-ray diffraction (XRD) measurements were performed on an XRD diffractonmeter (D8-Advance, Bruker, Germany). The patterns of Cu Kα radiation (λ = 0.15418 nm) at 40 kV and 30 mA were recorded in the 2θ region from 6 to 70° at a scanning speed of 2°/min. The crystallinity index (CI, %) of cellulose in the RC and RCZ films was calculated using the following equation:[40]

$$\mathrm{CI} = 100 \times \frac{I_{020} - I_{\mathrm{am}}}{I_{020}} \quad (1)$$

where I_{020} is the maximum intensity of the principal peak (020) lattice diffraction (2θ = 21.7° for cellulose II) and I_{am} is the intensity of diffraction attributed to amorphous cellulose (2θ = 16° for cellulose II). The average grain sizes (*D*) of ZnO nanoparticles in the RCZ films were calculated using the Debye−Scherrer equation:[41]

$$D = K\lambda(\beta\cos\theta)^{-1} \quad (2)$$

where λ is the wavelength of the X-ray radiation (Cu Kα = 0.15418 nm), *K* is the constant taken as 0.89, β is the line width at half-maximum height, and θ is the diffracting angle. X-ray photoelectron spectra (XPS) were recorded using an ESCALAB 250Xi (Thermo Scientific) X-ray photoelectron spectrometer with monochromatic Al Kα (1486.6 eV) radiation as the excitation source. The binding energy charge was corrected to 284.6 eV for C 1s.

DOI: 10.1021/am507639b
ACS Appl. Mater. Interfaces 2015, 7, 2597−2606

Scheme 2. Schematic Model Illustrating of the Formation of RCZ Films via One-Step Coagulation

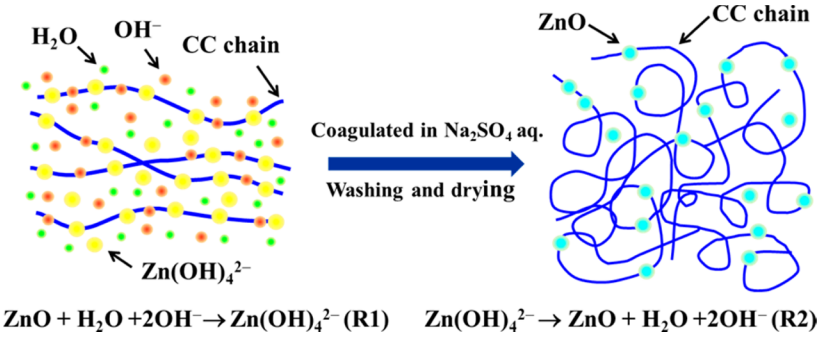

Table 1. Results of X-ray Diffraction, Tensile Testing, Wettability, and Antibacterial Activity Test with RC and RCZ Films[a]

	ZnO content (wt %)				d_{SEM} (μm)						W_{inh} (mm)	
sample	W_1	W_2	CI (%)	D (nm)	surface	cross-section	A_w (deg)	σ_b (MPa)	ε_b (%)	E (GPa)	*E. coli*	*S. aureus*
RC	0	0	66				79.7 (2.8)	40.6 (3.2)	11.1 (2.9)	2.5 (0.13)	0	0
RCZ4	6.4	2.7	66	15.3	1.0 (0.4)	1.1 (0.5)	87.5 (5.8)	55.0 (3.5)	10.1 (1.8)	3.0 (0.31)	5.8 (2.1)	8.7 (1.0)
RCZ8	12.1	7.4	61	16.4	1.6 (0.7)	1.5 (0.6)	96.2 (4.5)	57.1 (4.4)	10.1 (2.1)	3.1 (0.18)	7.2 (2.7)	9.7 (0.9)
RCZ12	17.1	11.7	57	18.2	2.1 (1.2)	1.9 (0.8)	103.4 (3.6)	49.0 (3.3)	10.6 (2.3)	2.7 (0.33)	8.8 (1.6)	12.3 (1.5)
RCZ16	21.6	15.1	55	19.2	2.4 (1.4)	2.1 (0.9)	102.0 (3.2)	43.3 (4.1)	8.6 (2.5)	2.6 (0.32)	10.2 (1.5)	18.8 (1.2)

[a] W_1, the theoretical value; W_2, determined by the TG analysis; CI, crystallinity index of cellulose; D, the average grain size of ZnO nanoparticles calculated by XRD; d_{SEM}, the mean size of the ZnO aggregates calculated by SEM; σ_b, tensile strength; ε_b, elongation at break; E, Young's modulus; W_{inh}, width of the inhibition zone; A_w, the water contact angle.

SEM images were obtained on a Hitachi S-4800 microscope using the back scattered electron imaging (BSE) mode. The wet films were frozen in liquid nitrogen, immediately snapped, and then freeze-dried. The samples were sputtered with gold for SEM measurements. Energy dispersive X-ray spectroscopy analysis (EDS) being attached to SEM was used to analyze the composition of the films. Transmission electron microscopy (TEM), high-resolution TEM (HRTEM), and selected area electron diffraction (SAED) pattern were performed on a JEM 2010 FEF (UHR) microscope (JEOL, Japan) at 200 kV. RCZ8 and RCZ16 films were embedded in an epoxy resin, and ultrathin slices were obtained for TEM measurements by sectioning on an LKB-8800 ultratome.

The stability of RCZ films in acidic, neutral and alkaline media was determined in 0.1 mol/L of HCl, NaCl, and NaOH aqueous solutions, respectively. RCZ12 film (0.1 g) was immersed into the media solution (100 mL) and stirred at 25 °C. The Zn concentration of the media was determined by using an inductively coupled plasma optical emission spectrometry (ICP-OES) (Intrepid XSP Radial, Thermo, USA). The weight loss of ZnO ($Loss_{ZnO}$) for RCZ12 film could be calculated as following:

$$Loss_{ZnO} = \frac{c \times 81 \times 0.1}{c_0 \times w \times 65} \times 100\% \quad (3)$$

where c is the Zn concentration of the media (mg/L), c_0 is the ZnO content of RCZ12 film (mg/g), and w is the weight of RCZ film (g). The mechanical properties of the films were measured in dry state on a universal tensile tester (CMT 6503, Shenzhen SANS Test Machine Co. Ltd., Shenzhen, China) at a speed of 2 mm/min according to ISO527-3-1995 (E). Before testing, the films were allowed to rest for at least 1 week at 75% RH. Conditioning was achieved to ensure the equilibration of the water content in the films with that of the atmosphere (stabilization of the sample weight). Each test was repeated at least five times and the average value was reported.

Testing of Antibacterial Activity. The antibacterial activity of the RC and RCZ films was examined using the disc diffusion method and colony-forming count method for qualitative and quantitative analyses, respectively. The Gram-positive bacterium *Staphylococcus aureus* (*S. aureus*) and Gram-negative bacterium *Escherichia coli* (*E. coli*) were administered; the final concentrations of bacterium were 1.0 × 10^8 and 3.0 × 10^8 CFU/mL, respectively. The bacteria were all ATCC.

The disc diffusion method was performed using Luria–Bertani (LB) medium solid agar in Petri dishes. RC and RCZ films were cut into 6 mm pieces, sterilized by UV light, and placed on *S. aureus*-cultured agar and *E. coli*-cultured agar plates, which were then incubated at 37 °C for 24 h. After incubation, a bacterial inhibition zone formed around the film. The width of the inhibition zone (W_{inh}) was calculated using the following equation:[30]

$$W_{inh} = \frac{d_1 - d_2}{2} \quad (4)$$

where d_1 is the total diameter of the inhibition zone and the film and d_2 is the diameter of the film (6 mm).

In the colony-forming count method, three pieces of RC or RCZ films (1 cm × 1 cm) were sterilized by UV light and then immersed in 10 mL of the bacterial suspension in an Erlenmeyer flask. The solution was then shaken at 200 rpm at 37 °C. Viable cell counts of the bacteria were obtained using the surface spread plate method. At 0, 1, 3, and 6 h intervals, 0.2 mL of bacterial culture was taken from the flask and serial dilutions were repeated with PBS in each initial sample, respectively. Then 0.1 mL of diluent of the sample was spread onto solid growth agar plates. The plates were incubated at 37 °C for 24 h, and the number of viable cells was manually counted and then multiplied by the dilution factor.

RESULTS AND DISCUSSION

Fabrication of Cellulose Based ZnO Nanocomposite Films. Scheme 1 illustrates the preparation of RCZ films from CC-NaOH/ZnO solutions. After casting the CC-NaOH/ZnO solution on a glass board, the solution was immersed in a Na_2SO_4 aq bath. RCZ films were then successfully fabricated via one-step coagulation. A schematic presentation for the construction of RCZ films is proposed in Scheme 2. In the initial CC-NaOH/ZnO solution, the dissolved ZnO was present as $Zn(OH)_4^{2-}$ (reaction R1), which could form strong

DOI: 10.1021/am507639b
ACS Appl. Mater. Interfaces 2015, 7, 2597–2606

hydrogen bonding with CC to break the intermolecular hydrogen bonds of polymer. Moreover, the large steric hindrance of $Zn(OH)_4^{2-}$ increased the distance between the polymer chains.[35] During the coagulation process, the precursor $Zn(OH)_4^{2-}$ decomposed into ZnO seed crystals (reaction R2),[21,25,29] and the strong interchain interactions of the exposed chains led to the rapid self-aggregation of cellulose. The abundant $Zn(OH)_4^{2-}$ facilitated nucleation on the ZnO seed crystal and enhanced the growth of ZnO nanoparticles. Moreover, the presence of Na_2SO_4 in the coagulating bath allowed for the rapid regeneration of cellulose molecules. By varying the ZnO concentration of the solvent from 0.4 to 1.6 wt %, the ZnO content of the obtained RCZ films was in the range of 2.7−15.1 wt % (Table 1), as determined by TG analysis. Attributing to the exchange of solvent and coagulant during the coagulation, the obtained RCZ films demonstrated lower ZnO content than the theoretical value (6.4−21.6 wt %). Compared with the previous work, this method is facile, green, and economical due to the absence of organic reagents (DMF,[20,27] acetone,[20,27] triethanolamine,[19,26] and alcohols[25,29]). It could easily be applied to scale up production at a viscose film (cellophane) plant.

Structure and Morphology of the Films. Figure 1 shows the XRD patterns of the RC and RCZ films. RC films displayed

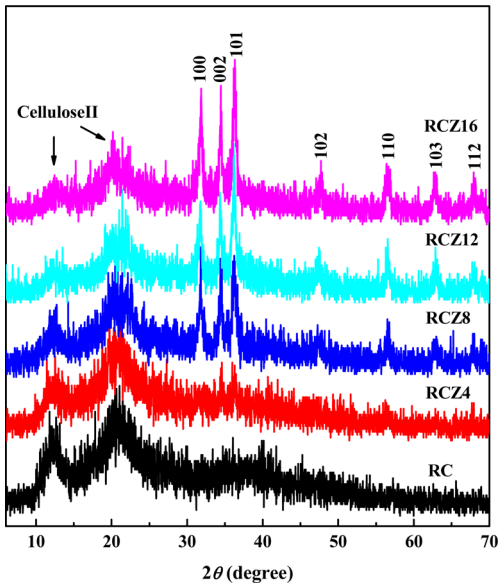

Figure 1. XRD patterns of the RC and RCZ films.

typical diffraction peaks at 2θ = 12, 20, and 22°, which were ascribed to the $(1\bar{1}0)$, (110), and (020) planes of the cellulose II crystalline form, respectively.[40] RCZ4 showed a similar pattern with RC except for two broad peaks at 2θ = 34.5 and 36.2°. In the RCZ8, RCZ12, and RCZ16 films, significant new peaks emerged at 2θ = 31.8, 34.5, 36.2, 47.8, 56.5, 62.8, and 68.0°, which corresponded to the (100), (002), (101), (102), (110), (103), and (112) planes of the ZnO crystal structure, respectively. All of the diffraction peaks were precisely indexed as a hexagonal wurtzite structure of ZnO (ICDD card no. 36-1451).[23,30,41] In addition, the diffraction peaks of ZnO were gradually strengthened with an increase of ZnO content. Characteristic peaks for impurity, such as $Zn(OH)_2$, were not observed, suggested that RCZ films were achieved without any impurities. The crystallinity index (CI) of cellulose II is summarized in Table 1. It was noted that the CI values of the films from RC to RCZ16 decreased from 66 to 55%, indicating that the crystalline structure of cellulose was partially destroyed by the ZnO nanoparticles. The average grain size of ZnO nanoparticles (Table 1), as determined from the 101 planes, increased slightly with increasing ZnO content in RCZ films and was in the range of 15.3−19.2 nm. The results clearly identified the successful attainment of cellulose/ZnO nanocomposite films through one-step coagulation.

FTIR spectra of the RC and RCZ films are shown in Figure 2. The peak at 1710 cm^{-1} in RC film was assigned to the

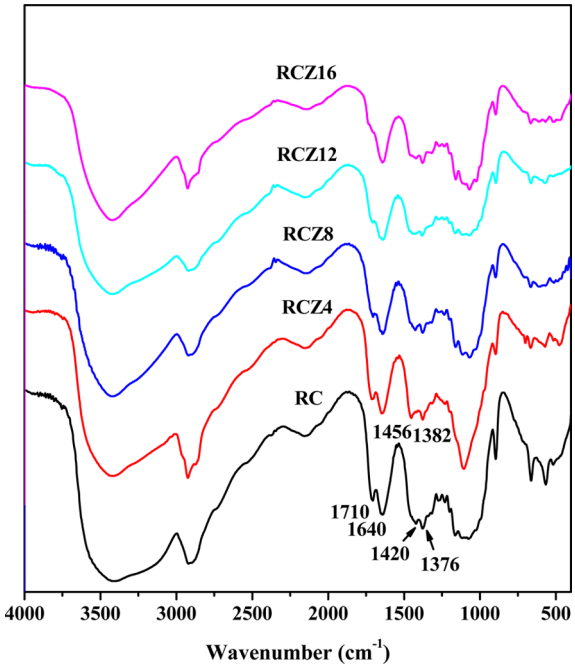

Figure 2. FTIR spectra of the RC and RCZ films.

stretching vibration of the carbonyl (C═O) in the base of urethane.[38] With the introduction of ZnO, the peak at 1710 cm^{-1} was weakened in RCZ4 film and almost disappeared in RCZ16 film. This could be ascribed to the hydrolysis of carbamate groups in the dissolving and regeneration processes with the introduction of zincate in the solvent. Moreover, the −OH stretching bands of cellulose at 1376 and 1420 cm^{-1} shifted to higher wavenumbers at 1382 and 1456 cm^{-1}, respectively, which confirmed the strong interaction between ZnO nanoparticles and cellulose chains.[20,42] The Zn−O vibration (~470 cm^{-1}) was not obvious in the spectra due to the low ZnO content of the nanocomposites.[30,42]

Figure 3 shows the wide-range XPS spectra of the RC, RCZ8, and RCZ16 films. RC film displayed two distinct peaks (C 1s and O 1s) in the binding energy spectra (Figure 3a). For RCZ8 and RCZ16 films, one pair of new peaks attributed to Zn 2p were observed, indicating the presence of ZnO at the outermost layer.[30] Figure 3b illustrates the curve fitting of the high-resolution multiplex scan spectra of the C 1s region. Three peaks at 284.8, 286.4, and 288.5 eV were observed for RC film, corresponding to the carbon of alkyl (C−C/C−H, absorbed), alcoholic/ether (C−O−C/C−OH), and carbonyl (C═O) of carbamate groups, respectively.[43] For RCZ8 and RCZ16 films, the peaks of alcoholic/ether demonstrated higher binding energy and were determined at 286.5 and 286.7 eV,

DOI: 10.1021/am507639b
ACS Appl. Mater. Interfaces 2015, 7, 2597−2606

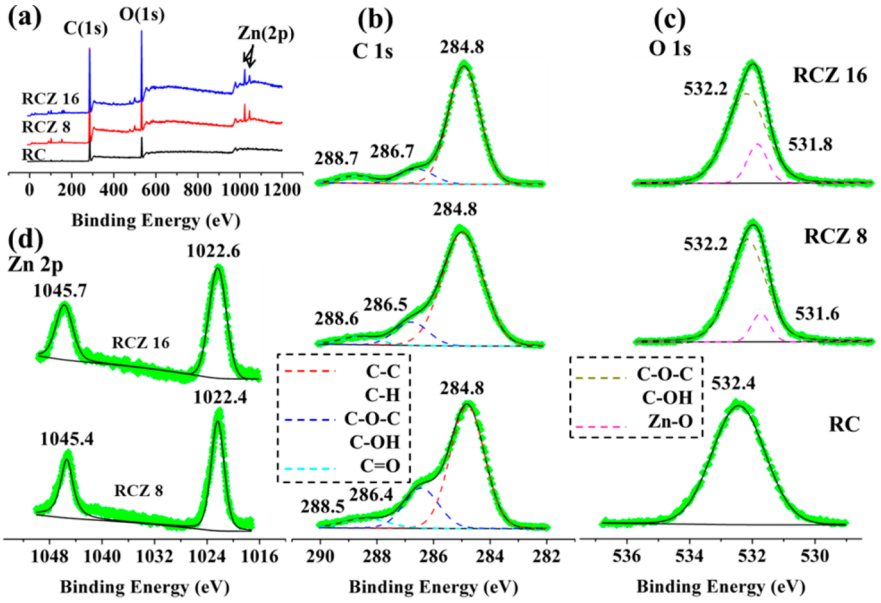

Figure 3. XPS spectra of the RC and RCZ films: (a) the wide-range spectra, (b) C 1s region, (c) O 1s region, and (d) Zn 2p region.

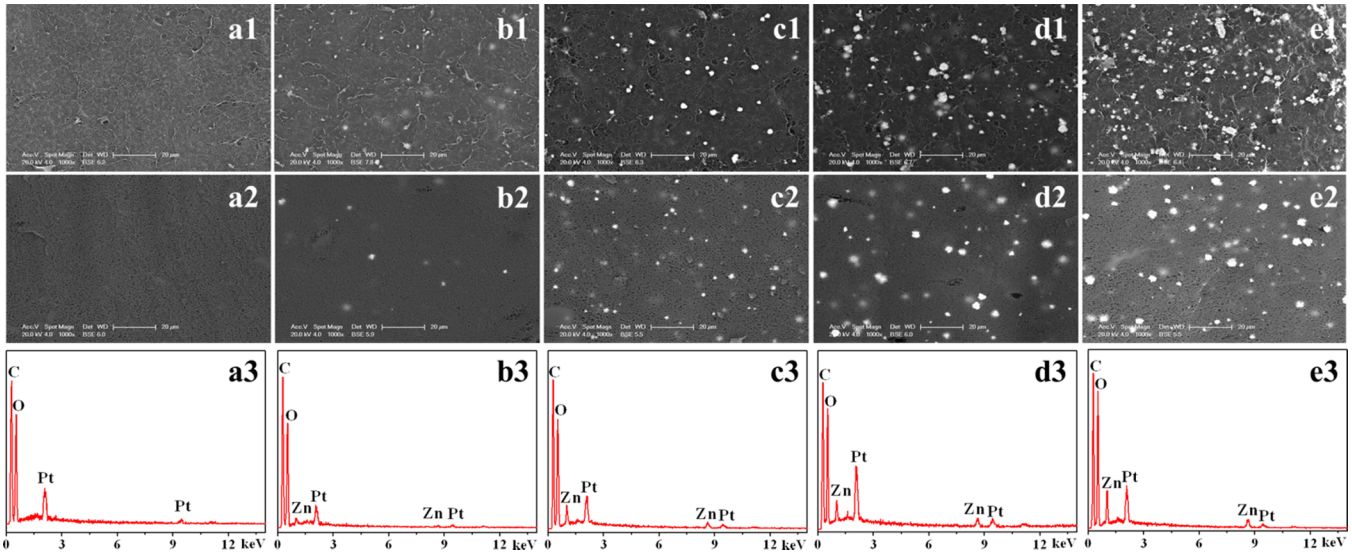

Figure 4. SEM images of the (a1−e1) surface and (a2−e2) cross-section of the films; (a3−e3) EDS spectra of the films: (a1, a2, a3) RC, (b1, b2, b3) RCZ4, (c1, c2, c3) RCZ8, (d1, d2, d3) RCZ12, (e1, e2, e3) RCZ16.

respectively. A similar phenomenon was observed in the carbonyl peaks and which shifted to a higher binding energy for RCZ16 (288.7 eV). The high resolution XPS spectra for the O 1s region are shown in Figure 3c. The peak at 532.4 eV for RC film was characteristic of the oxygen of alcoholic/ether (C−O−C/C−OH).[44] With the introduction of ZnO nanoparticles, the peak of alcoholic/ether shifted to a lower binding energy with a value at approximately 0.2 eV for RCZ8 and RCZ16 films. Moreover, new peaks for the O atoms of ZnO were observed in RCZ8 and RCZ16 films (531.6 and 531.8 eV, respectively). Figure 3d shows the high-resolution multiplex scan spectra of the Zn 2p region of RCZ films. The peaks at 1022.4 and 1022.6 eV corresponded to Zn 2p3/2, while the peaks at 1045.4 and 1045.7 eV were assigned to Zn 2p1/2. Interestingly, the binding energy of Zn 2p (2p3/2 and 2p1/2) shifted remarkably to higher binding energy (about 0.6 eV) compared with those of the ZnO nanofibers.[41] However, the observed spin−orbit splitting of Zn 2p (between Zn 2p3/2 and 2p1/2) for RCZ films was approximately 23 eV, which was consistent with the value of the pure ZnO nanoparticles, indicating a normal state of Zn^{2+} of ZnO in RCZ films.[41] Usually, binding energy shifts in XPS spectra can be attributed to two different kinds of mechanisms: the different electronegativities of metal ions and the strong interaction (electron transfer) between nanocrystals.[41] Therefore, the binding energy shifts for C 1s, O 1s, and Zn 2p proved the strong interaction between cellulose and ZnO nanoparticles in RCZ films.

Figure 4 shows the SEM images of the surface and cross-section of the films in BSE mode. RC film exhibited a dense and porous network structure. When the ZnO content increased from 2.7 to 15.1 wt %, more and more particles could be observed from the surface and inner-section of the RCZ films. ZnO particles on the surface aggregated to an irregular shape. As listed in Table 1, the mean size of the

DOI: 10.1021/am507639b
ACS Appl. Mater. Interfaces 2015, 7, 2597−2606

particles increased with increasing ZnO content. ZnO particles inside the films showed smaller size (1.1−2.1 μm) than those on the surface (1.0−2.4 μm). Generally, the polarity of water leads to the formation of agglomerated ZnO nanoparticles. However, the porous network of cellulose matrix prevented the diffusion of the precursor $[Zn(OH)_4^{2-}]$ to a certain extent and enabled better control of the growth of ZnO particles.[42] Therefore, the growth of ZnO particles inside the RCZ films was more uniform than the electrospinning method.[20] The EDS spectra of the films are shown in Figure 4a3−e3. Only C and O elements were present in the RC film, while C, O, and Zn were identified in all of the RCZ films. The wettability of the films was determined, and the results are summarized in Table 1. The water contact angle of RCZ films varied from 87.5° to 102.0° as the ZnO content increased, which was significantly larger than that of the RC film (79.7°). As shown in Figure 4, the surface morphology of the films became more and more rough with an increase of ZnO content. The interspaces among the ZnO particles could trap air whose water contact angle was considered as 180°.[45] Therefore, the trapped air could be served as part of the surface, resulting in a solid/air composite surface to increase the hydrophobicity of RCZ films.

Figure 5 shows the TEM images of the RCZ8 and RCZ16 films. The images depicted the uneven dispersion of ZnO

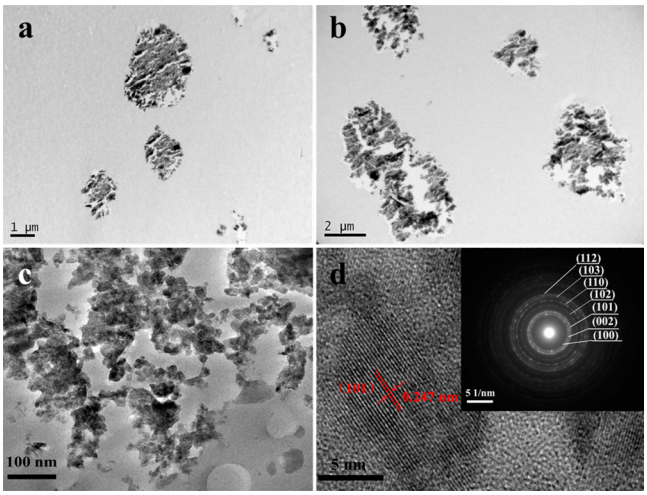

Figure 5. TEM images of (a) the RCZ8 and (b,c) RCZ16 films; (d) HRTEM image of the RCZ16 film, inset is the SAED pattern of the film.

particles in the cellulose matrix. It was evident that ZnO particles were formed through the close agglomeration of ZnO nanoparticles with a mean size of 18.6 nm (Figure 5c). This value was in agreement with the results calculated from the XRD analysis. ZnO nanoparticles in the RCZ16 film showed lattice spacing of 2.47 Å (Figure 5d), which was indexed to the (101) plane of the hexagonal wurtzite ZnO particle (ICDD card no. 36-1451). The inset image of Figure 5d shows the SAED pattern of the film. The calculated lattice constants were indexed to the (100), (002), (101), (102), (110), (103), and (112) planes of ZnO,[46] respectively, which were in accordance with the results of XRD.

Physical Properties of the Films. The stability of RCZ films in acidic, neutral, and alkaline media was determined. As the RCZ films immersed into 0.1 mol/L HCl solution, the white films changed to transparent immediately, indicating that ZnO particles were reacted with HCl and transferred into the soluble Zn^{2+}. However, the color of RCZ films in neutral and alkaline media exhibited no obvious changes after the treatment of 24 h. Figure 6 shows the weight loss of ZnO for RCZ12 films

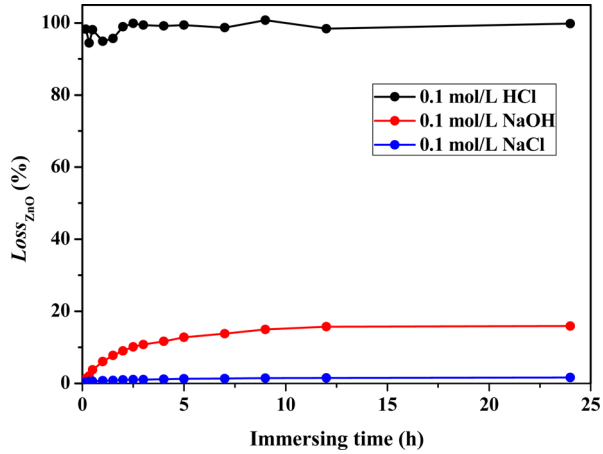

Figure 6. Dependence of the immersing time on the weight loss of ZnO ($Loss_{ZnO}$) for RCZ12 films in different media at 25 °C.

immersed into different media with various times. It was noted that about 98% of ZnO in the film was lost in 0.1 mol/L HCl aq within 10 min. The loss of ZnO in 0.1 mol/L NaOH aq increased with an increase of immersing time, and the $Loss_{ZnO}$ value was about 16% after 24 h. Though ZnO could react with NaOH to form the water-soluble $Zn(OH)_4^{2-}$, the strong interactions between $Zn(OH)_4^{2-}$ and cellulose resulted in the relatively slow loss of ZnO from the films.[35] The nanocomposite films displayed high stability in neutral media, and only 1.6% of the ZnO particles escaped from the matrix after the duration in 0.1 mol/L NaCl aq for 24 h.

Figure 7 shows the stress−strain curves of the films. RC film had good tensile strength (σ_b) and Young's modulus (E), with

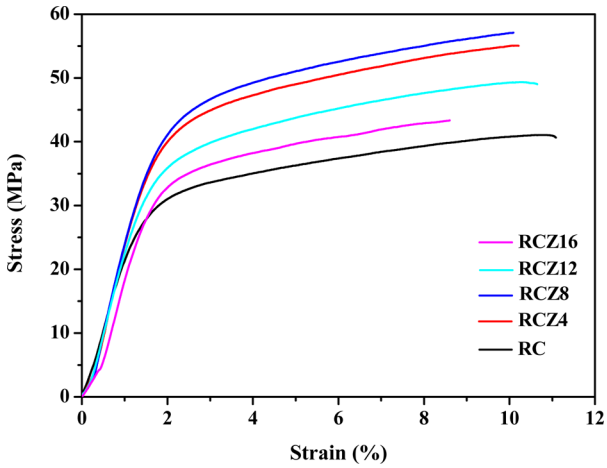

Figure 7. Stress−strain curves of the RC and RCZ films.

values of 40.6 MPa and 2.5 GPa, respectively. An increase in the ZnO content from 2.7 wt % (RCZ4) to 7.4 wt % (RCZ8) led to a slight decrease in the elongation at break (ε_b) of the RCZ films when compared with that of the RC film. However, the E and σ_b values slightly increased and reached 3.1 GPa and 57.1 MPa with 7.4 wt % ZnO loaded. The values are comparable with those of the cellulose−carbon nanotube film (E = 2.6 GPa

DOI: 10.1021/am507639b
ACS Appl. Mater. Interfaces 2015, 7, 2597−2606

and σ_b = 59.4 MPa).[47] The σ_b values of the films decreased with increased ZnO content over 7.4 wt %. A similar result was observed on cellulose−SiO_2 nanocomposite films[48] and cellulose/graphene oxide composite films.[49] This could be attributed to the tendency of ZnO nanoparticles to form larger agglomerates at higher content, leading to relatively poor dispersion in the cellulose matrix. However, all of the RCZ films displayed higher tensile strength than RC film, which further confirmed the strong interactions between ZnO nanoparticles and cellulose matrix.

Figure 8 illustrates the TG and differential thermogravimetry (DTG) curves of the films under an air atmosphere. A small amount of weight loss was observed below 100 °C, which was assigned to the release of moisture from the films.[15] RC film showed two obvious weight loss steps under elevated temperature. The first weight loss step occurred in the temperature range of 280−350 °C, which was attributed to the onset of cellulose decomposition.[15] The second weight loss peak occurred at 350−610 °C and was ascribed to the full decomposition of cellulose.[15] RCZ films exhibited similar thermal decomposition process but demonstrated lower complete degradation temperature (ca. 620 °C) than that of RC film (ca. 690 °C). This could be attributed to the catalyst properties of ZnO nanoparticles, which facilitated faster breakdown of the cross-linking in the carbon skeleton.[23]

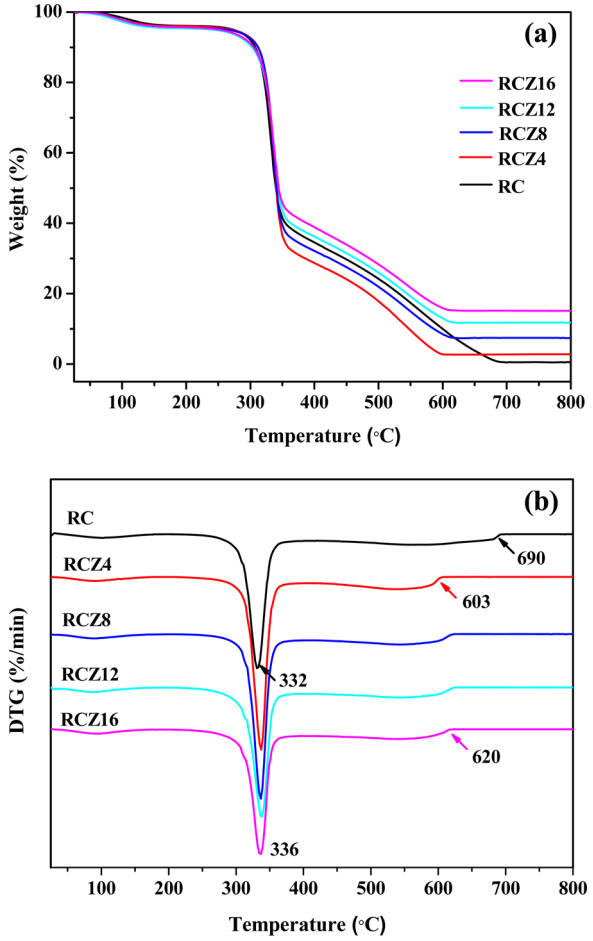

Figure 8. (a) TG and (b) DTG curves of the RC and RCZ films under an air atmosphere.

Figure 9a shows the UV−vis absorption spectra of the films. RCZ films with higher ZnO content (RCZ8, RCZ12, and RCZ16) clearly demonstrated a peak at 360 nm. The spectra of RCZ films were similar to that of cellulose−ZnO composites prepared from a wet chemical method (350 nm)[26] and cellulose−ionic liquid solution (358 nm).[23] This suggested that the ZnO particles in the composites were roughly the same size.[41] RC film did not show any major absorption peaks in the same spectral region. ZnO absorption peaks were not observed in the spectrum of RCZ4 films, which was attributed to its relatively lower ZnO content. The band gap energy of the ZnO nanoparticles was calculated according the following equation:[41]

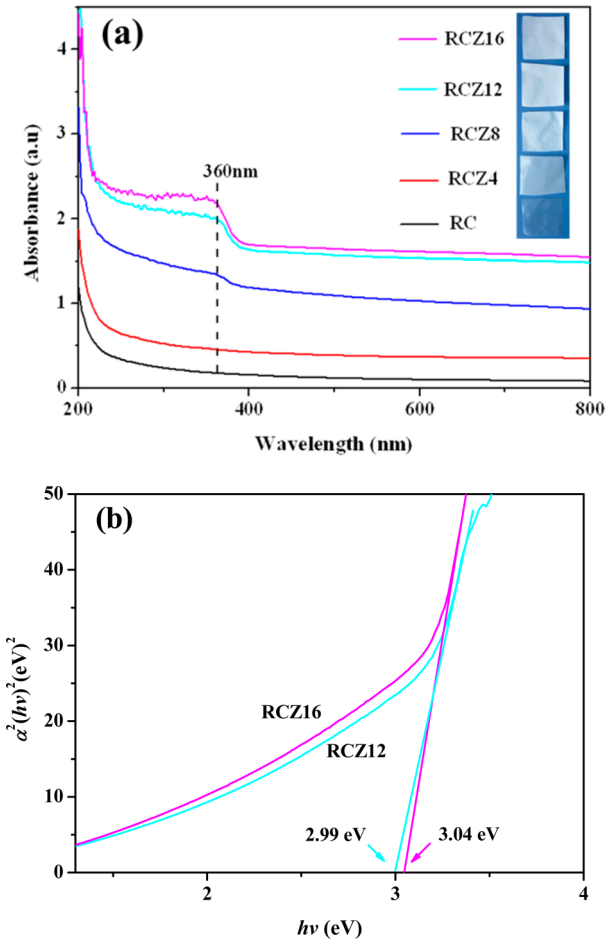

Figure 9. (a) UV−visible spectra and (b) the energy band gap of the RC and RCZ films.

$$\alpha h\nu = A(h\nu - E_g)^{n/2} \quad (5)$$

where α, ν, E_g, and A is the absorption coefficient, light frequency, band gap, and constant, respectively. Moreover, n depends on the characteristics of the semiconductor transition: direct transition (n = 1) or indirect transition (n = 4). For ZnO, the value of n is 1 for the direct transition. Therefore, the band gap energy of the ZnO nanoparticles in RCZ films could be estimated from a plot of $(\alpha h\nu)^2$ versus photon energy $h\nu$. As shown in Figure 9b, the band gap of ZnO for RCZ12 and RCZ16 films was determined as 2.99 and 3.04 eV, respectively, which was similar to the pure ZnO nanoparticles (3.22 eV).[41]

DOI: 10.1021/am507639b
ACS Appl. Mater. Interfaces 2015, 7, 2597−2606

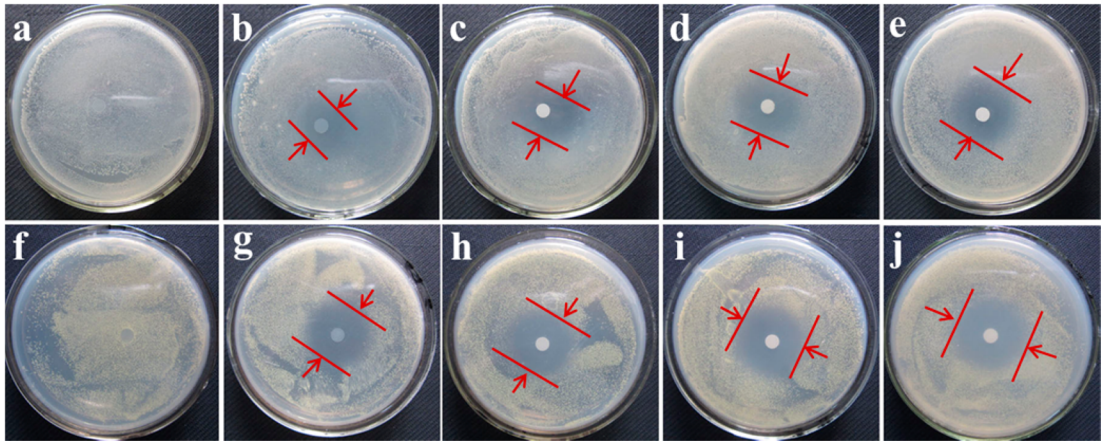

Figure 10. Inhibition zone test of the RC and RCZ films against (a–e) *E. coli* and (f–j) *S. aureus*: (a,f) RC, (b,g) RCZ4, (c,h) RCZ8, (d,i) RCZ12, (e,j) RCZ16.

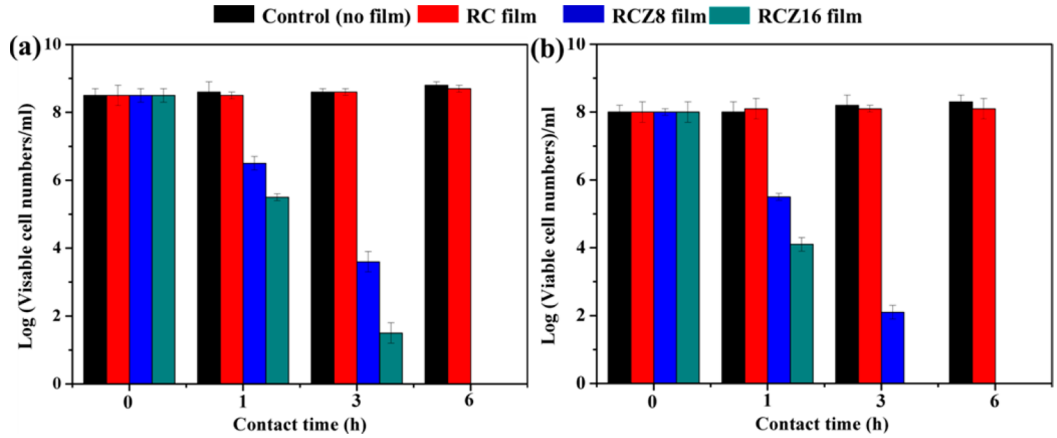

Figure 11. Viable cell numbers of (a) *E. coli* and (b) *S. aureus* in the control group, RC, RCZ8, and RCZ16 films with different contact time.

The results suggested that RCZ films had enhanced UV-blocking properties compared to the RC film.

Antibacterial Properties. Figure 10 shows the inhibition zone test of the films against *E. coli* and *S. aureus*. RC films did not indicate any detectable inhibition zones. In contrast, significant inhibition zones were observed for RCZ films. As summarized in Table 1, the width of the inhibition zone around RCZ films showed significant growth with increased ZnO content for both *S. aureus* and *E. coli* after 1 day, varying in the range of 8.7–18.8 mm and 5.8–10.2 mm, respectively. Moreover, the nanocomposite films demonstrated a stronger influence on *S. aureus* than *E. coli*. The results are in agreement with previously reported literature.[20,50,51] The nature of the cell wall structure is one of the possible reasons for different sensitivity.[20] *S. aureus* is composed of multilayers of peptidoglycan with an abundant amount of pores that renders them more susceptible to reactive species, leading to cell disruption. The cell wall of *E. coli* is relatively thin and is mainly comprised of peptidoglycan, while the outer layer consists of lipopolysaccharide, lipoprotein, and phospholipids, which would be less vulnerable to the attack of a reactive species. Therefore, RCZ films displayed better antibacterial activity against *S. aureus* than *E. coli*.

The antibacterial properties of RCZ films were also quantitatively evaluated using the colony-forming count method (Figure 11). RC films did not demonstrate any antibacterial activity for *E. coli* and *S. aureus*, and the number of viable bacteria remained static. However, a 2-log reduction and 3-log reduction in the viable bacteria of *E. coli* were observed within 1 h of exposure in RCZ8 and RCZ16 films (Figure 11a), respectively. When the contact time increased to 3 h, a more significant reduction in the viable bacteria of *E. coli* was observed for RCZ8 (5-log) and RCZ16 films (7-log). After 6 h of exposure, the *E. coli* bacteria were completely eradicated. As shown in Figure 11b, RCZ films showed more rapid sterilization for *S. aureus* than *E. coli*. After 1 h of treatment, a 2.5-log and 4-log reduction was observed for *S. aureus* in RCZ8 and RCZ16 films, respectively, and a 100% reduction in viability was reached after 3 h for the RCZ16 film. Enhanced antibacterial properties were identified in RCZ films compared to ZnO nanostructures-deposited cotton fabrics[51] and chitosan–ZnO-based cotton fabric.[52] This could be attributed to the porous structure of RCZ films and the enhanced dispersion stability of ZnO nanoparticles in the cellulose matrix.[20] The porous structure provided empty space that allowed the water molecules to react with the incorporated ZnO nanoparticles, leading to the generation of reactive species, such as oxy-radical or hydroxyl-radical species.[10,30,51,52]

These reactive species caused oxidative injury inside the bacterial cells, resulting in excellent antibacterial activities of RCZ films.

DOI: 10.1021/am507639b
ACS Appl. Mater. Interfaces 2015, 7, 2597–2606

CONCLUSIONS

Cellulose based ZnO nanocomposite films were successfully prepared from CC-NaOH/ZnO aqueous solutions through one-step coagulation. With an increase of ZnO concentration from 0.4 to 1.6 wt % in the solvent, the ZnO content of the nanocomposites increased from 2.7 to 15.1 wt %. ZnO nanoparticles with the size of 15−19 nm agglomerated into large particles with the size of 1.0−2.4 μm, which were firmly embedded in the cellulose matrix. The strong interactions occurred between ZnO particles and cellulose matrix in the RCZ films. The tensile strength and Young's modulus of RCZ films were enhanced with the incorporation of ZnO nanoparticles. RCZ films displayed good UV-blocking properties and high stability in neutral media. Particularly, RCZ films exhibited excellent antibacterial activities against *E. coli* and *S. aureus*. A dramatic reduction in viable bacteria was observed within 3 h of exposure and all of the bacteria were eliminated within 6 h. Therefore, RCZ films have significant potential for application in biomedical, catalysis, packaging, and electronic fields.

AUTHOR INFORMATION

Corresponding Author

*Fax: (+) 86-27-68754067. E-mail: zhoujp325@whu.edu.cn.

Notes

The authors declare no competing financial interest.

ACKNOWLEDGMENTS

This work was financially supported by National Natural Science Foundation of China (51273151), Program for New Century Excellent Talents in University (NCET-11-0415), and the Open Project of State Key Laboratory Cultivation Base for Nonmetal Composites and Functional Materials (12ZXFK03).

REFERENCES

(1) Sun, Y.; Seo, J. H.; Takacs, C. J.; Seifter, J.; Heeger, A. J. Inverted Polymer Solar Cells Integrated with a Low-Temperature-Annealed Sol-Gel-Derived ZnO Film as an Electron Transport Layer. *Adv. Mater.* **2011**, *23*, 1679−1683.

(2) Mu, J.; Shao, C.; Guo, Z.; Zhang, Z.; Zhang, M.; Zhang, P.; Chen, B.; Liu, Y. High Photocatalytic Activity of ZnO−Carbon Nanofiber Heteroarchitectures. *ACS Appl. Mater. Interfaces* **2011**, *3*, 590−596.

(3) Xiao, Y.; Lu, L.; Zhang, A.; Zhang, Y.; Sun, L.; Huo, L.; Li, F. Highly Enhanced Acetone Sensing Performances of Porous and Single Crystalline ZnO Nanosheets: High Percentage of Exposed (100) Facets Working Together with Surface Modification with Pd Nanoparticles. *ACS Appl. Mater. Interfaces* **2012**, *4*, 3797−3804.

(4) Wu, J.; Xue, D. Progress of Science and Technology of ZnO as Advanced Material. *Sci. Adv. Mater.* **2011**, *3*, 127−149.

(5) Perelshtein, I.; Applerot, G.; Perkas, N.; Wehrschetz-Sigl, E.; Hasmann, A.; Guebitz, G. M.; Gedanken, A. Antibacterial Properties of an In Situ Generated and Simultaneously Deposited Nanocrystalline ZnO on Fabrics. *ACS Appl. Mater. Interfaces* **2009**, *1*, 363−366.

(6) Xu, S.; Wang, Z. One-Dimensional ZnO Nanostructures: Solution Growth and Functional Properties. *Nano Res.* **2011**, *4*, 1013−1098.

(7) Singh, D. P. Synthesis and Growth of ZnO Nanowires. *Sci. Adv. Mater.* **2010**, *2*, 245−272.

(8) Kumar, P. T. S.; Lakshmanan, V. K.; Anilkumar, T. V.; Ramya, C.; Reshmi, P.; Unnikrishnan, A. G.; Nair, S. V.; Jayakumar, R. Flexible and Microporous Chitosan Hydrogel/Nano ZnO Composite Bandages for Wound Dressing: In Vitro and in Vivo Evaluation. *ACS Appl. Mater. Interfaces* **2012**, *4*, 2618−2629.

(9) Applerot, G.; Abu-Mukh, R.; Irzh, A.; Charmet, J.; Keppner, H.; Laux, E.; Guibert, G.; Gedanken, A. Decorating Parylene-Coated Glass with ZnO Nanoparticles for Antibacterial Applications: A Comparative Study of Sonochemical, Microwave, and Microwave-Plasma Coating Routes. *ACS Appl. Mater. Interfaces* **2010**, *2*, 1052−1059.

(10) Manna, J.; Begum, G.; Kumar, K. P.; Misra, S.; Rana, R. K. Enabling Antibacterial Coating via Bioinspired Mineralization of Nanostructured ZnO on Fabrics under Mild Conditions. *ACS Appl. Mater. Interfaces* **2013**, *5*, 4457−4463.

(11) Siro, I.; Plackett, D. Microfibrillated Cellulose and New Nanocomposite Materials: A Review. *Cellulose* **2010**, *17*, 459−494.

(12) Klemm, D.; Heublein, B.; Fink, H. P.; Bohn, A. Cellulose: Fascinating Biopolymer and Sustainable Raw Material. *Angew. Chem., Int. Ed.* **2005**, *44*, 3358−3393.

(13) Olsson, R. T.; Samir, M.; Salazar-Alvarez, G.; Belova, L.; Strom, V.; Berglund, L. A.; Ikkala, O.; Nogues, J.; Gedde, U. W. Making Flexible Magnetic Aerogels and Stiff Magnetic Nanopaper Using Cellulose Nanofibrils as Templates. *Nature Nanotechnol.* **2010**, *5*, 584−588.

(14) Chen, L.; Huang, Z.; Liang, H.; Guan, Q.; Yu, S. Bacterial-Cellulose-Derived Carbon Nanofiber@MnO_2 and Nitrogen-Doped Carbon Nanofiber Electrode Materials: An Asymmetric Supercapacitor with High Energy and Power Density. *Adv. Mater.* **2013**, *25*, 4746−4752.

(15) Jia, B.; Mei, Y.; Cheng, L.; Zhou, J.; Zhang, L. Preparation of Copper Nanoparticles Coated Cellulose Films with Antibacterial Properties through One-Step Reduction. *ACS Appl. Mater. Interfaces* **2012**, *4*, 2897−2902.

(16) Mahmoud, K. A.; Lam, E.; Hrapovic, S.; Luong, J. H. T. Preparation of Well-Dispersed Gold/Magnetite Nanoparticles Embedded on Cellulose Nanocrystals for Efficient Immobilization of Papain Enzyme. *ACS Appl. Mater. Interfaces* **2013**, *5*, 4978−4985.

(17) Kumar, A.; Gullapalli, H.; Balakrishnan, K.; Botello-Mendez, A.; Vajtai, R.; Terrones, M.; Ajayan, P. M. Flexible ZnO−Cellulose Nanocomposite for Multisource Energy Conversion. *Small* **2011**, *7*, 2173−2178.

(18) Costa, S. V.; Goncalves, A. S.; Zaguete, M. A.; Mazon, T.; Nogueira, A. F. ZnO Nanostructures Directly Grown on Paper and Bacterial Cellulose Substrates without Any Surface Modification Layer. *Chem. Commun.* **2013**, *49*, 8096−8098.

(19) Cheng, F.; Betts, J. W.; Kelly, S. M.; Wareham, D. W.; Kornherr, A.; Dumestre, F.; Schaller, J.; Heinze, T. Whiter, Brighter, and More Stable Cellulose Paper Coated with Antibacterial Carboxymethyl Starch Stabilized ZnO Nanoparticles. *J. Mater. Chem. B* **2014**, *2*, 3057−3064.

(20) Anitha, S.; Brabu, B.; Thiruvadigal, D. J.; Gopalakrishnan, C.; Natarajan, T. S. Optical, Bactericidal and Water Repellent Properties of Electrospun Nanocomposite Membranes of Cellulose Acetate and ZnO. *Carbohydr. Polym.* **2013**, *97*, 855−855.

(21) Khatri, V.; Halasz, K.; Trandafilovic, L. V.; Dimitrijevic-Brankovic, S.; Mohanty, P.; Djokovic, V.; Csoka, L. ZnO-Modified Cellulose Fiber Sheets for Antibody Immobilization. *Carbohydr. Polym.* **2014**, *109*, 139−147.

(22) Gimenez, A. J.; Yanez-Limon, J. M.; Seminario, J. M. ZnO−Cellulose Composite for UV Sensing. *IEEE Sens. J.* **2013**, *13*, 1301−1306.

(23) Bagheri, M.; Rabieh, S. Preparation and Characterization of Cellulose−ZnO Nanocomposite Based on Ionic Liquid ($[C_4mim]Cl$). *Cellulose* **2013**, *20*, 699−705.

(24) Martins, N. C. T.; Freire, C. S. R.; Neto, C. P.; Silvestre, A. J. D.; Causio, J.; Baldi, G.; Sadocco, P.; Trindade, T. Antibacterial Paper Based on Composite Coatings of Nanofibrillated Cellulose and ZnO. *Colloids Surf., A* **2013**, *417*, 111−119.

(25) Bhatti, H. S.; Kumar, S.; Singh, K. Structural and Optical Characterization of Hydroxy-Propyl Methyl Cellulose-Capped ZnO Nanorods. *J. Mater. Sci.* **2013**, *48*, 5536−5542.

(26) John, A.; Ko, H. U.; Kim, D. G.; Kim, J. Preparation of Cellulose−ZnO Hybrid Films by a Wet Chemical Method and Their Characterization. *Cellulose* **2011**, *18*, 675−680.

(27) Ye, S.; Zhang, D.; Liu, H.; Zhou, J. ZnO Nanocrystallites/Cellulose Hybrid Nanofibers Fabricated by Electrospinning and

DOI: 10.1021/am507639b
ACS Appl. Mater. Interfaces 2015, 7, 2597−2606

Solvothermal Techniques and Their Photocatalytic Activity. *J. Appl. Polym. Sci.* **2011**, *121*, 1757−1764.
(28) Goncalves, G.; Marques, P.; Neto, C. P.; Trindade, T.; Peres, M.; Monteiro, T. Growth, Structural, and Optical Characterization of ZnO-Coated Cellulosic Fibers. *Cryst. Growth Des.* **2009**, *9*, 386−390.
(29) Wang, R.; Xin, J.; Tao, X.; Daoud, W. ZnO Nanorods Grown on Cotton Fabrics at Low Temperature. *Chem. Phys. Lett.* **2004**, *398*, 250−255.
(30) Katepetch, C.; Rujiravanit, R.; Tamura, H. Formation of Nanocrystalline ZnO Particles into Bacterial Cellulose Pellicle by Ultrasonic-Assisted in Situ Synthesis. *Cellulose* **2013**, *20*, 1275−1292.
(31) Ghule, K.; Ghule, A. V.; Chen, B.; Ling, Y. Preparation and Characterization of ZnO Nanoparticles Coated Paper and Its Antibacterial Activity Study. *Green Chem.* **2006**, *8*, 1034−1041.
(32) Li, C.; Liu, Q.; Shu, S.; Xie, Y.; Zhao, Y.; Chen, B.; Dong, W. Preparation and Characterization of Regenerated Cellulose/TiO_2/ZnO Nanocomposites and Its Photocatalytic Activity. *Mater. Lett.* **2014**, *117*, 234−236.
(33) Bazant, P.; Kuritka, I.; Munster, L.; Machovsky, M.; Kozakova, Z.; Saha, P. Hybrid Nanostructured Ag/ZnO Decorated Powder Cellulose Fillers for Medical Plastics With Enhanced Surface Antibacterial Activity. *J. Mater. Sci.: Mater. Med.* **2014**, *25*, 2501−2512.
(34) Nagaraju, G.; Ko, Y. H.; Yu, J. Facile Synthesis of ZnO/CuO Nanostructures on Cellulose Paper and Their p−n Junction Properties. *Mater. Lett.* **2014**, *116*, 64−67.
(35) Fu, F.; Guo, Y.; Wang, Y.; Tan, Q.; Zhou, J.; Zhang, L. Structure and Properties of the Regenerated Cellulose Membranes Prepared from Cellulose Carbamate in NaOH/ZnO Aqueous Solution. *Cellulose* **2014**, *21*, 2819−2830.
(36) Fu, F.; Zhou, J.; Zhou, X.; Zhang, L.; Li, D.; Kondo, T. Green Method for the Production of Cellulose Multifilament from Cellulose Carbamate on a Pilot-Scale. *ACS Sustainable Chem. Eng.* **2014**, *2*, 2363−2370.
(37) Fu, F.; Yang, Q.; Zhou, J.; Hu, H.; Jia, B.; Zhang, L. Structure and Properties of Regenerated Cellulose Filaments Prepared from Cellulose Carbamate−NaOH/ZnO Aqueous Solution. *ACS Sustainable Chem. Eng.* **2014**, *2*, 2604−2612.
(38) Guo, Y.; Zhou, J.; Song, Y.; Zhang, L. An Efficient and Environmentally Friendly Method for the Synthesis of Cellulose Carbamate by Microwave Heating. *Macromol. Rapid Commun.* **2009**, *30*, 1504−1508.
(39) Guo, Y.; Zhou, J.; Zhang, L. Dynamic Viscoelastic Properties of Cellulose Carbamate Dissolved in NaOH Aqueous Solution. *Biomacromolecules* **2011**, *12*, 1927−1934.
(40) French, A. D. Idealized Powder Diffraction Patterns for Cellulose Polymorphs. *Cellulose* **2014**, *21*, 885−896.
(41) Zhang, Z.; Shao, C.; Li, X.; Wang, C.; Zhang, M.; Liu, Y. Electrospun Nanofibers of p-Type NiO/n-Type ZnO Heterojunctions with Enhanced Photocatalytic Activity. *ACS Appl. Mater. Interfaces* **2010**, *2*, 2915−2923.
(42) Hu, W.; Chen, S.; Zhou, B.; Wang, H. Facile Synthesis of ZnO Nanoparticles Based on Bacterial Cellulose. *Mater. Sci. Eng., B* **2010**, *170*, 88−92.
(43) You, J.; Zhao, C.; Cao, J.; Zhou, J.; Zhang, L. Fabrication of High-Density Silver Nanoparticles on the Surface of Alginate Microspheres for Application in Catalytic Reaction. *J. Mater. Chem. A* **2014**, *2*, 8491−8499.
(44) Gorjanc, M.; Jazbec, K.; Šala, M.; Vesel, A.; Mozetič, M. Creating Cellulose Fibres with Excellent UV Protective Properties Using Moist CF_4 Plasma and ZnO Nanoparticles. *Cellulose* **2014**, *21*, 3007−3021.
(45) He, M.; Xu, M.; Zhang, L. Controllable Stearic Acid Crystal Induced High Hydrophobicity on Cellulose Film Surface. *ACS Appl. Mater. Interfaces* **2013**, *5*, 585−591.
(46) Lin, B.; Shen, P.; Chen, S. ZnO and epsilon-$Zn(OH)_2$ Composite Nanoparticles by Pulsed Laser Ablation on Zn in Water. *J. Phys. Chem. C* **2011**, *115*, 5003−5010.
(47) Qi, H.; Liu, J.; Gao, S.; Mader, E. Multifunctional Films Composed of Carbon Nanotubes and Cellulose Regenerated from Alkaline−Urea Solution. *J. Mater. Chem. A* **2013**, *1*, 2161−2168.
(48) Song, H.; Zheng, L. Nanocomposite Films Based on Cellulose Reinforced with Nano-SiO_2: Microstructure, Hydrophilicity, Thermal Stability, and Mechanical Properties. *Cellulose* **2013**, *20*, 1737−1746.
(49) Huang, H.; Liu, C.; Li, D.; Chen, Y.; Zhong, G.; Li, Z. Ultra-low Gas Permeability and Efficient Reinforcement of Cellulose Nanocomposite Films by Well-Aligned Graphene Oxide Nanosheets. *J. Mater. Chem. A* **2014**, *2*, 15853−15863.
(50) Wang, Y.; Du, G.; Liu, H.; Liu, D.; Qin, S.; Wang, N.; Hu, C.; Tao, X.; Jiao, J.; Wang, J.; Wang, Z. Nanostructured Sheets of Ti-O Nanobelts for Gas Sensing and Antibacterial Applications. *Adv. Funct. Mater.* **2008**, *18*, 1131−1137.
(51) Singh, G.; Joyce, E. M.; Beddow, J.; Mason, T. J. Evaluation of Antibacterial Activity of ZnO Nanoparticles Coated Sonochemically onto Textile Fabrics. *J. Microbiol. Biotechnol. Food Sci.* **2012**, *2*, 106−120.
(52) Perelshtein, I.; Ruderman, E.; Perkas, N.; Tzanov, T.; Beddow, J.; Joyce, E.; Mason, T. J.; Blanes, M.; Mollá, K.; Patlolla, A. Chitosan and Chitosan−ZnO-Based Complex Nanoparticles: Formation, Characterization, and Antibacterial Activity. *J. Mater. Chem. B* **2013**, *1*, 1968−1976.

DOI: 10.1021/am507639b
ACS Appl. Mater. Interfaces 2015, 7, 2597−2606